ANL-77-90

ANL-77-90

A STUDY OF THE PRODUCTION OF WELL-CHARACTERIZED AEROSOLS USING A FLOW REACTOR

by

Roger W. Zygmunt

ARGONNE NATIONAL LABORATORY, ARGONNE, ILLINOIS

Prepared for the U. S. DEPARTMENT OF ENERGY
under Contract W-31-109-Eng-38

Printed in the United States of America
Available from
National Technical Information Service
U. S. Department of Commerce
5285 Port Royal Road
Springfield, Virginia 22161
Price: Printed Copy $4.50; Microfiche $3.00

Distribution Category:
Chemistry (UC-4)

ANL-77-90

ARGONNE NATIONAL LABORATORY
9700 South Cass Avenue
Argonne, Illinois 60439

A STUDY OF THE PRODUCTION OF WELL-CHARACTERIZED AEROSOLS USING A FLOW REACTOR

by

Roger W. Zygmunt

Chemical Engineering Division

December 1977

TABLE OF CONTENTS

LIST OF FIGURES

LIST OF TABLES

NOMENCLATURE

D_p	particle diameter, μm
g	gravitational acceleration, cm/s^2
K_o	coagulation constant, cm^3/s
l	tube length, m
n	number concentration at the tube exit (equivalent particle concentration), $particles/cm^3$
n_o	inlet number concentration, $particles/cm^3$
p	atmospheric pressure, torr
R	radius of the tube, cm
t	time, h
V_f	mean flow velocity in the tube, cm/s
V_p	volume of air necessary to "purge" the flow reactor, liters
V_s	particle settling velocity, cm/s
ρ_p	particle density, g/cm^3
ρ_f	density of fluid medium, g/cm^3
μ_f	coefficient of viscosity of the fluid medium, g/(cm)(s)

A STUDY OF THE PRODUCTION OF WELL-CHARACTERIZED AEROSOLS USING A FLOW REACTOR

by

Roger W. Zygmunt

ABSTRACT

A flow reactor system is being used to produce well-characterized aerosols reproducible in terms of particle size distribution, chemical composition, and concentration. These aerosols are generated by passing air through glass frits immersed in appropriate solutions, with the flow reactor serving as an aging chamber for the aerosol.

A neutral ammonium sulfate [$(NH_4)_2SO_4$] aerosol was the first to be characterized. The particle size distribution was measured by means of an optical counter, with the measurements showing that most of the aerosol particles were in the 0.5-0.7 μm size range. The chemical composition of the aerosol was determined by infrared spectroscopy, and the concentration was determined from the mass flow rate. A mass balance calculation indicated that the mass loss of aerosol in transit through the flow reactor was 23.0 ± 3.5%. This loss was attributed largely to sedimentation. The effects of diffusional deposition and coagulation were found to be negligible.

Five factors affecting the aerosol generation in a glass frit bubbler system were investigated. Particle concentration increased as the solution concentration increased and as the solution height above the frit decreased. The type of frit used to generate the aerosol influenced particle size distribution, with coarse frits producing an increased concentration of the larger particle sizes. As the flow rate of air through the frit increased, the particle concentration also increased. Below 70% relative humidity, no effect on the particle size distribution of neutral ammonium sulfate aerosol was observed with variation in relative humidity.

Attempts to generate organic and metal-bearing aerosols were only partly successful.

I. INTRODUCTION

An important aspect of the environmental pollution problem concerns sulfate aerosols, which are known to have adverse effects on public health and welfare. Because of the effects, it is becoming increasingly apparent that the sulfate aerosols and their effects on health must be examined more closely than in the past.[1]

Natural sulfur emissions, such as biological decomposition or salt water spray, are believed to account for about two-thirds of the total sulfur emissions (222 million tons per year) on a global basis.[2]

Hydrogen sulfide resulting from biological decay accounts for about 100 million tons of this sulfur. It is believed that the H_2S is rapidly oxidized to sulfate in the atmosphere. Sea salt spray accounts for 43 million tons per year of sulfur emissions. Most of this sea salt never reaches the global land masses but is deposited in the sea. The remaining 79 million tons per year of sulfur originates from industrial sources. A breakdown of this figure shows that about one million tons of this sulfur are emitted as sulfate compounds (primarily H_2SO_4 and metal sulfates), while the remainder comprises 75 million tons of SO_2 and 3 million tons of H_2S. In the United States, anthropogenic sulfur emissions far outweigh the contribution from natural sources.[3]

Sulfate in aerosols, which is derived in large part through the oxidation of gaseous sulfur emissions, can exist in a number of different chemical forms. These include, in the order of increasing abundance, organic sulfates, metallic sulfates, sulfuric acid, and acid and neutral ammonium sulfates.[4,5] Available toxicological reports indicate that sulfuric acid and sulfate aerosols are more potent irritants than sulfur dioxide,[6] and the U.S. Environmental Protection Agency expects to establish a National Ambient Air Quality Standard for sulfates by 1981.[7]

Animal toxicology, rather than human epidemiology, is being emphasized as a basis for establishing standards because of the inherent problems associated with epidemiologic studies. To carry out controlled studies, toxicologists need a dependable system that can generate and deliver well-characterized aerosols to an animal exposure chamber. An aerosol of known size distribution, chemical composition, and concentration would constitute a well-characterized aerosol. Currently, a flow reactor for generating such aerosols is being studied for possible use as an integral part of such a system. The Biological and Medical Research Division (BIM) at Argonne National Laboratory has proposed utilization of a scaled-up version of the flow reactor used in the present study to generate aerosols for use in animal toxicological studies.

II. AMBIENT AEROSOL SIZE DISTRIBUTION

Figure 1 represents the size distribution of typical ambient aerosol in Pasadena, California, as construed by Whitby *et al.*[8] The area under any portion of the curves is proportional to the concentration of aerosol in that particular size range. At the bottom of the figure, the principal mechanisms affecting growth and removal of particles in each size range are indicated. The short dashed lines are extrapolations and, as such, were not constructed from actual data. The data indicate that the particles present in the greatest number lie in the 0.002 to 0.02-μm size range, whereas those with the greatest surface area lie in the 0.05 to 0.5-μm size range. The aerosol volume or mass exhibits a bimodal distribution.

This bimodal character of the aerosol volume distribution may not be so pronounced if the atmosphere sampled had not been a photochemical type smog atmosphere.[8] Fifty percent of the aerosol mass is contained in the size range $0.05 \leq D_p \leq 1.05$ μm (where D_p is the particle diameter), whereas only 5% of the particle number is present in the same size range. The

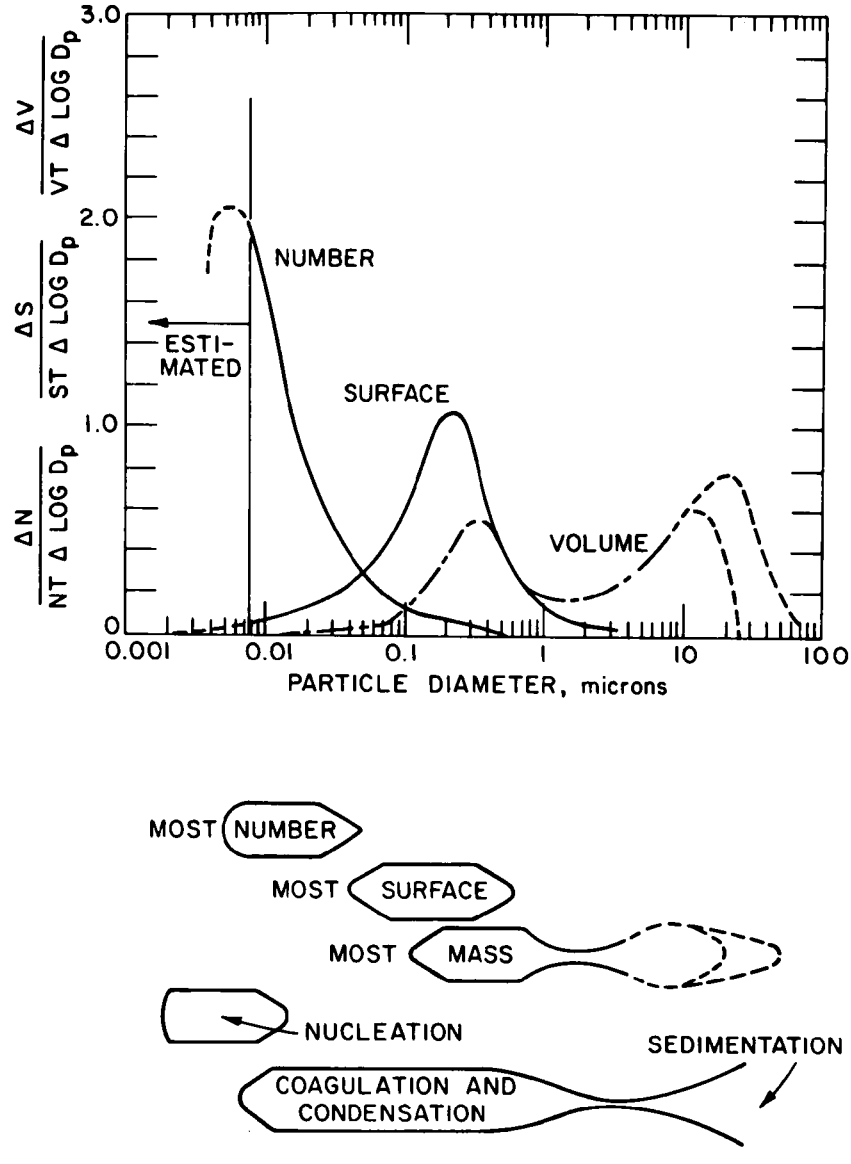

Fig. 1. Size Distribution of Atmospheric Particles

particles in this size range result from the coagulation of particles less than 0.05 μm in diameter and from the condensation of photochemical reaction products on submicrometer-sized aerosol. The mass of particles in the size range $D_p > 1.05$ μm is only weakly coupled with the mass in the $D_p < 1.0$ μm range and originates from large-particle emissions, windborne dust, and sea spray, as well as through coagulation of smaller particles. The bimodal characteristic of the volume distribution results from an accumulation of mass in the $0.1 \leq D_p \leq 0.8$-μm size range as a result of coagulation and condensation of smaller particles and a separate accumulation of mass in the $2.0 \leq D_p \leq 8$-μm size range due to equilibration between sources of larger particles and sedimentation.

"Accumulation mode" is the term assigned to the 0.1 to 1.0-μm size range.[9] It is here that the contribution of secondary particles (those formed in the atmosphere through gas-to-particle conversion processes) dominates. Fully 80% of the ambient sulfate is found in the accumulation mode.[10] Particles in the accumulation mode are of a size that is most effective in scattering light; thus, they have a direct bearing on visibility reduction in the ambient atmosphere.[9] Since the deposition velocity for unit density aerosol reaches a minimum between 0.1 and 1.0 μm,[10] it can be concluded that removal of sulfate by dry deposition on the ground and other surfaces is relatively slow.

III. HEALTH EFFECTS

Laboratory studies have shown that ambient concentrations of submicron sulfates can irritate the trachea, bronchia and bronchioles.[11] Epidemiologic studies have shown that, when sulfate levels exceed 10 $\mu g/m^3$, the frequency of asthma attacks in susceptible humans increases.[12] Epidemiologic data indicate that, if the levels remain above 13 $\mu g/m^3$ for several years, lower respiratory disease probably increases in children.

Animal toxicology studies are focusing on the health effects of sulfate aerosols. Sulfuric acid aerosols have been shown to cause inflammation and subsequent constriction of bronchial airways within the respiratory tract.[13,14] Particle size and relative humidity both govern the irritant potency of sulfated aerosols.[15] Studies with zinc ammonium sulfate aerosol showed that it is a greater irritant than zinc sulfate or ammonium sulfate, but less than sulfuric acid.[16] From a toxicological point of view, it is apparent from these preliminary studies that the submicrometer-sized sulfate aerosols, in particular neutral and acidic ammonium sulfate aerosols, must be examined in greater detail.

Organic compounds present in particulate material in the atmosphere have been studied primarily for their possible carcinogenic effects in animals and man.[17] Incomplete combustion is the major source of a large number of these organic compounds present in the ambient air.[18] Secondary reactions in the atmosphere may increase the number of condensable organic compounds in the environment.

IV. EXPERIMENTAL

For this study, a flow reactor was used to produce and condition, through aging, a sulfate aerosol. The flow reactor system consisted of three parts: (1) an aerosol generation portion, (2) an aging portion, and (3) a downstream monitoring portion. The sulfate aerosol was generated using bubblers in which air was distributed by glass frits. A 3.5-m-long glass pipe with a volume of about 0.064 m^3 was used to condition and age the aerosol, and an optical particle counter monitored the downstream size distribution. Samples were collected at the reactor exit for chemical analysis. In addition to sulfate aerosol, metal aerosols and organic aerosols were also generated using appropriate techniques. Chemical characterization was achieved using X-ray diffraction, atomic absorption, gas chromatographic, and infrared spectrophotometric techniques.

Figure 2 is a schematic diagram of the aerosol generator and flow reactor assembly. The reactor itself is made of Corning Pyrex pipe, 152-mm ID, connected by metal collars with teflon gaskets sealing the joints. The reactor is 3.5 m in length formed from two 1.52-m-long pipe sections separated by a 0.46-m-long tee-section to provide for mid-point sampling. Baffles are provided at the inlet to minimize turbulence. The front end plate to which the gas dispersion apparatus is connected is constructed of 13-mm-thick mild steel. The rear end plate is constructed of 13-mm-thick Type 304 stainless steel. Under normal operation, compressed air is passed through a filter and a bed of molecular sieves before entering the flow reactor system. The filter, 0.8 μm pore size Millipore, removes particulate matter and the molecular sieves remove gaseous impurities from the compressed air. After being cleaned, the air stream passes through two humidification bubblers before entering the final bubbler filled with an appropriate solution to generate the desired aerosol. The aerosol-laden air then passes through teflon tubing to one of the gas dispersion tubes at the inlet end of the flow reactor. The air stream has a residence time of about 15 min in the flow reactor. After passing through the flow reactor, a small portion of the air stream is routed to the Royco, Model 225, particle counter. After adding an appropriate amount of clean make-up air, the stream then passes through a Casella impactor and a final Millipore filter. The impactor and filter were used for collecting samples for infrared spectroscopic, X-ray diffraction and atomic absorption spectrophotometric analyses.

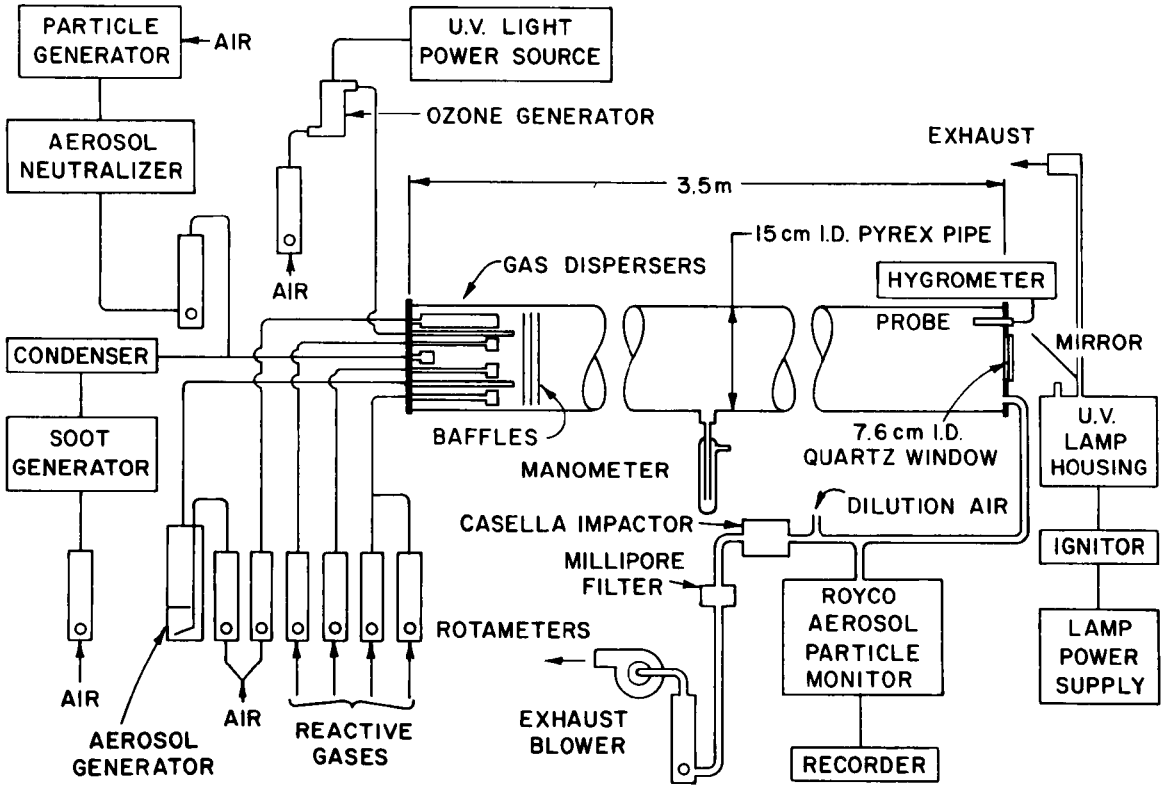

Fig. 2. Schematic Diagram of the Flow Reactor

Two independent physical processes are involved in the generation of aerosols by gas dispersion flasks.[19] Bubbles are formed by the air as it passes through the frit and these rise to the surface of the liquid. Upon penetrating the surface, a bubble assumes a dome shape. Owing to a reduction in surface tension, constituents such as $(NH_4)_2SO_4$ present in the solution tend to stabilize the bubble, retarding the thinning of the film at the dome apex due to liquid drainage. Eventually, the dome apex ruptures and a high velocity gas jet formed from positive pressure within the bubble shatters the bubble film, providing the mechanism for the formation of very small film droplets. A jet of liquid is ejected from the crater formed beneath the liquid surface within the dome. This jet disintegrates into droplets that are much larger than the film droplets and represents the second aerosol formation mechanism. The number of film droplets formed is proportional to the diameter of the dome, while the number of jet droplets formed decreases with increasing bubble diameter. For air bubbles in water less than 0.5 mm in diameter, a few film droplets are formed but a large number of jet droplets can be expected. For bubbles greater than 6.0 mm in diameter, few jet droplets will be produced because the jet ejection velocities are very low. For bubbles whose diameters lie between 0.5 mm and 6.0 mm, a bimodal distribution consisting of large jet droplets and small film droplets is produced. Film droplets become more uniform in size as the bubble diameter increases. However, the jet droplets are generally more monodisperse than the film droplets. Thus, monodispersity of the size distribution is enhanced by the formation of jet droplets from very small bubbles. However, when the bubbles are generated, they tend to coalesce after reaching the solution surface. In the flow reactor generation scheme used in this work, coarse frits were used to produce a mixture of large and small bubbles. This resulted in a mixture of film and jet droplets, constituting a polydisperse aerosol with a size range of from <0.5 μm to about 10.0 μm in diameter.

Metal aerosols were generated by burning an alcoholic solution of the metal acetates contained in an alcohol lamp. Organic aerosols were produced through sublimation and subsequent condensation of the organic material in the presence of a noncondensable carrier gas.

V. RESULTS

To characterize the ammonium sulfate aerosol in the flow reactor system, it was necessary to establish the size distribution, concentration, and chemical composition of the aerosol. A Royco, Model 225, particle counter was used to obtain upstream and downstream ammonium sulfate aerosol size distributions. Infrared spectroscopy and X-ray diffraction were used to determine the chemical composition of the ammonium sulfate aerosol. Atomic absorption spectroscopy and gas chromatographic analyses were used to determine the composition of the metal aerosol and organic aerosol, respectively.

A. Mass Balance

As a first step in the characterization of ammonium sulfate aerosol in the flow reactor system, a mass balance encompassing the entire flow reactor was conducted. By comparing the mass of $(NH_4)_2SO_4$ aerosol entering and leaving the flow reactor, wall losses and sample line losses were determined.

The Millipore filters used to collect the aerosol particles had a pore size of 1.0 μm. A 250 cm^3 bubbler equipped with a relatively coarse glass frit (maximum pore diameter, 40-60 μm) was used to produce the aerosol. In each trial 100 cm^3 of a 0.05M $(NH_4)_2SO_4$ solution (Research Chemical Corp. ultra-pure grade, 99.99%) was used in the bubbler.

Data for the mass balance experiment are presented in Table 1. The average $(NH_4)_2SO_4$ mass flow rate entering the reactor (point B. Fig. 2) was 0.143 ± 0.029 mg/h. This corresponds to a concentration of 597 ± 121 μg $(NH_4)_2SO_4/m^3$ of air. The average $(NH_4)_2SO_4$ mass flow rate leaving the reactor (point A, Fig. 2) was 0.11 ± 0.017 mg/h, which represented a total mass loss within the flow reactor of 23 ± 3.5%. The average mass flow rate leaving the reactor corresponds to a concentration of 459 ± 72 μg $(NH_4)_2SO_4/m^3$.

B. Aerosol Size Distribution

As a second step in the characterization of ammonium sulfate aerosol in the flow reactor system, the optical particle counter was used to obtain size distributions of the aerosol. Figure 3 and Table 2 provide data representative of the upstream and downstream size distributions. The downstream data were obtained with the particle counter connected as shown in Fig. 2. To obtain the upstream data, the particle counter sample line was connected to the aerosol bubbler system at point B (Fig. 2).

Three general observations can be made relative to these data. First, Fig. 3 shows that about 90% of the particles exist in the size range <1.4 μm, with about 60% being less than 0.7 μm in diameter. Second, Table 2 indicates that the $(NH_4)_2SO_4$ particle concentrations decrease with increasing particle diameter. Finally, there is a decrease in particle concentration between the entry and exit of the flow reactor. In addition to deposition of particles by sedimentation, drying of the wet aerosol within the flow reactor contributes to this decrease. Further, as the indicated particle diameter increases, the percent loss becomes greater. This is probably due to deposition of the particles by sedimentation.

Once equilibrium was established in the flow reactor, both the upstream and downstream particle size distributions remained stable with time. The theoretical time necessary to reach equilibrium was calculated to be 1.23 h at an air flow rate of 4.0 L/min. The approximate experimental time to reach equilibrium was one hour, with the equilibrium being determined by a steady reading from the optical particle counter.

The magnitudes of particle removal by diffusion, sedimentation, and coagulation in the flow reactor were calculated theoretically. These calculations are included in the Appendix. The decrease in particle concentration due to diffusional deposition on the walls of the flow reactor was calculated from a nomograph (Fig. 6.8, Ref. 20). As a result of these calculations, it was concluded that diffusional deposition effects in the flow reactor can be neglected. Removal of particles by sedimentation in the flow reactor is not negligible, however. The gravitational settling loss of particles flowing through the flow reactor was calculated from the following equation:[20]

Table 1. Mass Balance across the Flow Reactor[a]

	Entering the Flow Reactor			Leaving the Flow Reactor		
	Trial 1	Trial 2	Trial 3	Trial 4	Trial 5	Trial 6
Mass Gain on the Filter, mg	0.70	1.00	1.00	0.50	0.80	0.60
Time, h	6.17	6.25	6.22	5.12	6.00	6.00
$(NH_4)_2SO_4$ Mass Flow Rate, mg/h	0.11±0.007	0.16±0.11	0.16±0.011	0.10±0.007	0.13±0.009	0.10±0.007
	Avg. 0.143 ± 0.029			Avg. 0.11 ± 0.017		
$(NH_4)_2SO_4$ Concentration, $\mu g/m^3$	458±29	667±458	667±46	417±29	542±38	417±29
	Avg. 597 ± 121			Avg. 459 ± 72		

[a]The air flow rate through the bubblers was 2.0 L/min, with an additional 2.0 L air/min added at the reactor inlet.

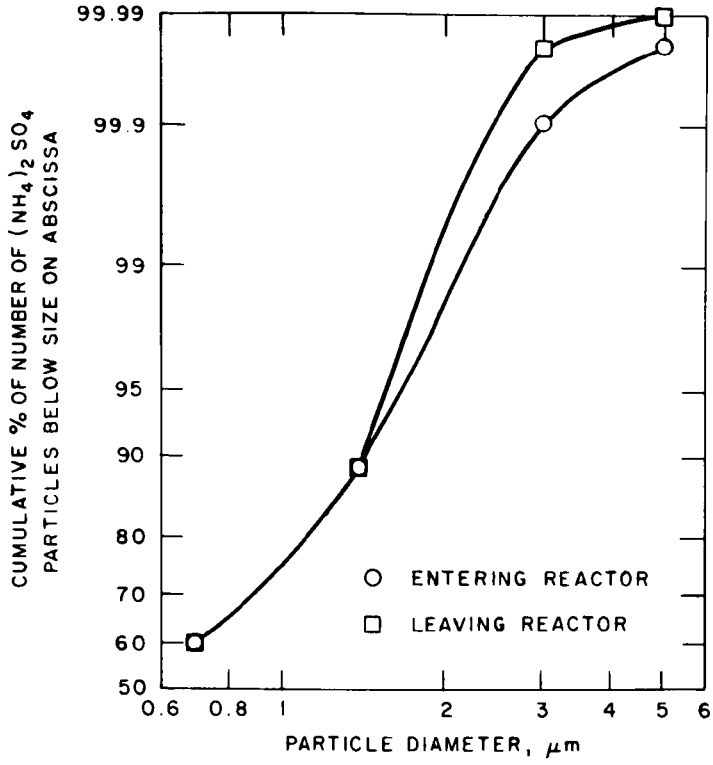

Fig. 3. Size Distribution of $(NH_4)_2SO_4$ Particles Entering and Leaving the Flow Reactor in the Mass Balance Experiment

Table 2. Size Distribution of $(NH_4)_2SO_4$ Particles Entering and Leaving the Flow Reactor in the Mass Balance Experiment (Selected Data)

	Size Range, μm	Equivalent Particle Concentration, particles/cm^3
Entering Flow Reactor[a]	>0.5	205.0
	>0.7	81.2
	>1.4	20.8
	>3.0	0.18
	>5.0	0.04
Leaving Flow Reactor[b]	>0.5	201.0
	>0.7	77.7
	>1.4	18.7
	>3.0	0.04
	>5.0	0.02

[a]These data were taken at 1.5 h run time.

[b]These data were taken at 4.0 h run time.

$$n/n_o = \exp\left[\frac{-2V_s l}{\pi V_f R}\right] \quad (1)$$

For example, for 0.7-μm dia particles, a loss of particles of about 11.2% occurs between the inlet and outlet owing to deposition by sedimentation. The magnitude of particle removal by coagulation in the flow reactor was calculated from the following equation:[21]

$$\frac{1}{n} - \frac{1}{n_o} = K_o t \quad (2)$$

As a result of these calculations, it can be concluded that particle coagulation in the flow reactor was negligible in the size range which the particle counter can measure (*i.e.*, $0.5 \leq D_p \leq 10.0$ μm).

C. Infrared Spectroscopy

As a final step in the characterization of ammonium sulfate aerosol in the flow reactor system, infrared spectroscopy was used to identify the chemical composition of the aerosol obtained in these experiments. Infrared spectra of $(NH_4)_2SO_4$ and NH_4HSO_4 are presented in Figs. 4 and 5, respectively. The top spectrum in Fig. 4 is that of a sample of 0.05M $(NH_4)_2SO_4$ solution evaporated to dryness on a hot plate. Three features of interest are the NH_4^+ peak at 1400 cm^{-1}, and the two neutral sulfate peaks at 1110 and 620 cm^{-1}. The bottom spectrum in Fig. 4 is that of an impactor-collected aerosol sample taken at the exit port of the flow reactor and generated with 0.05M $(NH_4)_2SO_4$ solution in the bubbler. The three primary peaks for the ammonium and sulfate ions correlate well with the first spectrum.

The top spectrum in Fig. 5 is that of a sample of 0.05M NH_4HSO_4 solution evaporated to dryness on a hot plate. In this instance, five features are of interest: the NH_4^+ peak at 1400 cm^{-1} and the acid sulfate peaks at 1205, 1080, 880, and 600 cm^{-1}. The NH_4HSO_4 aerosol was generated by placing a 0.05M NH_4HSO_4 solution in the bubbler and using nitrogen as the carrier gas in the flow reactor. An impactor-collected sample at the exit port of the flow reactor yielded an infrared spectrum which correlated well with the spectrum obtained with the dried NH_4HSO_4.

D. Factors Affecting Aerosol Characteristics

Several aspects of aerosol generation in the bubbler system were investigated. These included the effect of solution concentration, solution height above the frit, frit type, air flow rate through the frit, and humidity on the aerosol particle size distribution and number concentration of ammonium sulfates. In order to investigate these factors, a base case of variables was established, defined as follows: bubbler flow rate of 2.0 L air/min, dilution air 2.0 L/min, the top of the coarse frit (maximum pore size 40-60 μm in diameter) 32 mm below the solution surface, 100 mL volumes of 0.05M $(NH_4)_2SO_4$ to be used in each trial, and a relative humidity of 50% (figured arithmetically from the humidified and dry air flow rates except for the experiments concerning the effect of humidity).

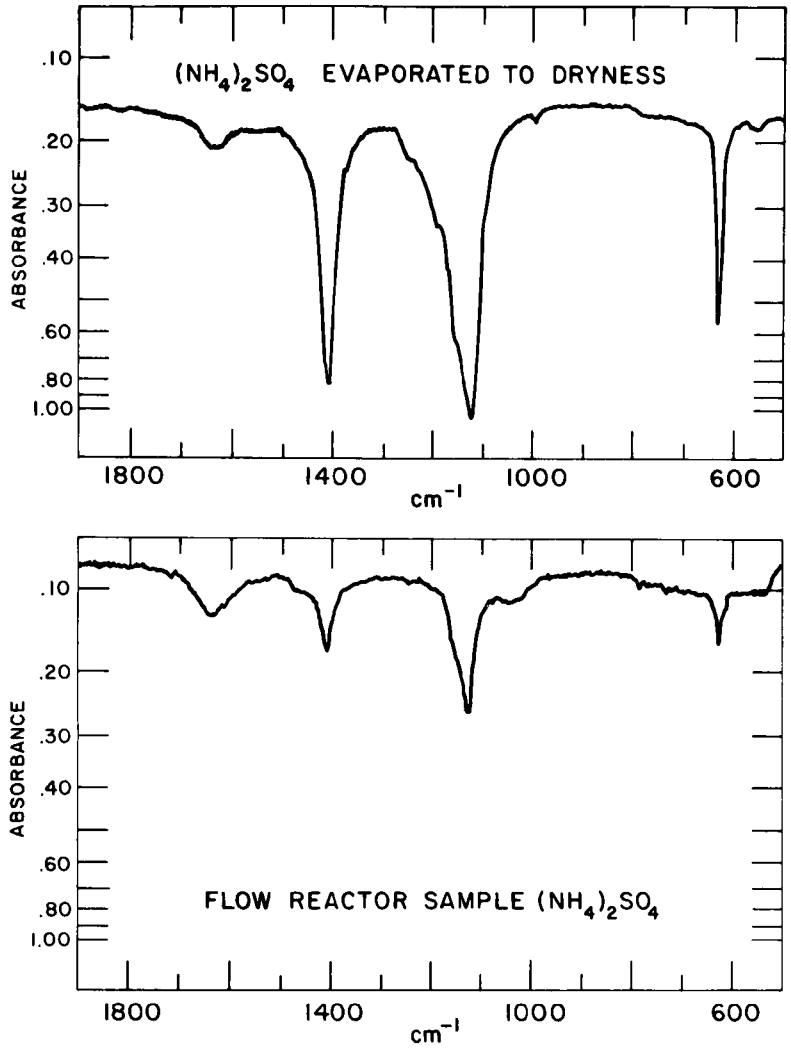

Fig. 4. Infrared Spectra of $(NH_4)_2SO_4$

Concentration was varied from the base case of 5×10^{-2} to 5×10^{-7}M $(NH_4)_2SO_4$. In Fig. 6, the $(NH_4)_2SO_4$ concentration in the solution is plotted *vs.* the equivalent particle concentration calculated from the particle counter data (on logarithmic scales). In general, as the solution concentration increases, the equivalent particle concentration also increases, with the sharpest increase occurring in the 5×10^{-3} to 5×10^{-2}M concentration range. For the curves $D_p > 0.7$ μm and $D_p > 1.4$ μm, a plateau is reached in the concentration range from 5×10^{-5} to 5×10^{-3}M. The plateau was reproducible and shows that the relationship between the log of the equivalent particle concentration and the log of the $(NH_4)_2SO_4$ concentration is not strictly linear.

Solution height above the frit was varied from 0-70 mm. Figure 7 shows the bubbler in detail. The frit is mounted in a downward 30-degree plane from the horizontal. Height above the solution is measured from the point where this imaginary plane intersects a horizontal plane at the top of the

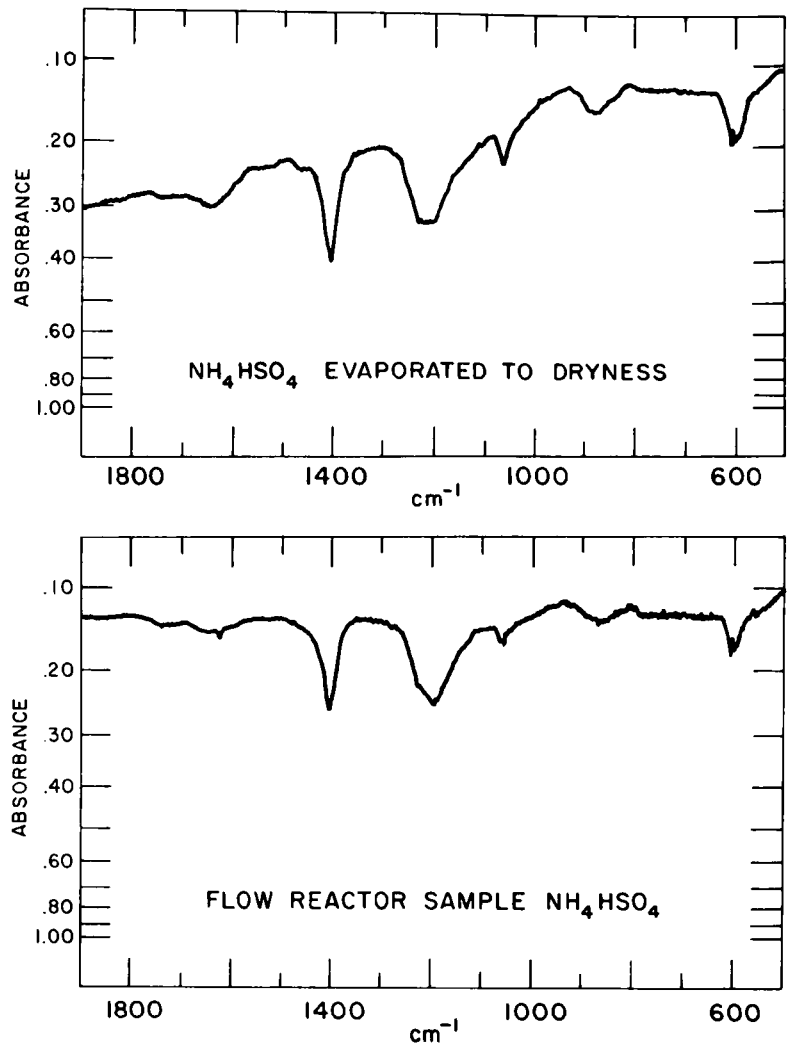

Fig. 5. Infrared Spectra of NH_4HSO_4

frit. Thus, at a height of zero mm of solution above the frit, the frit is still completely immersed in the solution. Solution height would be expected to have an effect on particle size distribution because it affects phenomena occurring while the bubble is rising. In Fig. 8, a plot of the solution height above the frit *vs.* the equivalent particle concentration calculated from the particle counter data is presented. Figure 8 indicates that the equivalent particle concentration decreases linearly as the solution height above the frit increases. This can be accounted for by the fact that an increased solution depth results in more time for the bubbles to coalesce and thus decrease the final aerosol concentration since with coalescence fewer bubbles would be bursting at the solution surface. Theoretically, this effect should be most pronounced in the smallest bubble size because coalescence increases as the bubble size decreases. Experimentally, this is also the case since the curve for particle diameters >0.5 μm has the steepest slope.

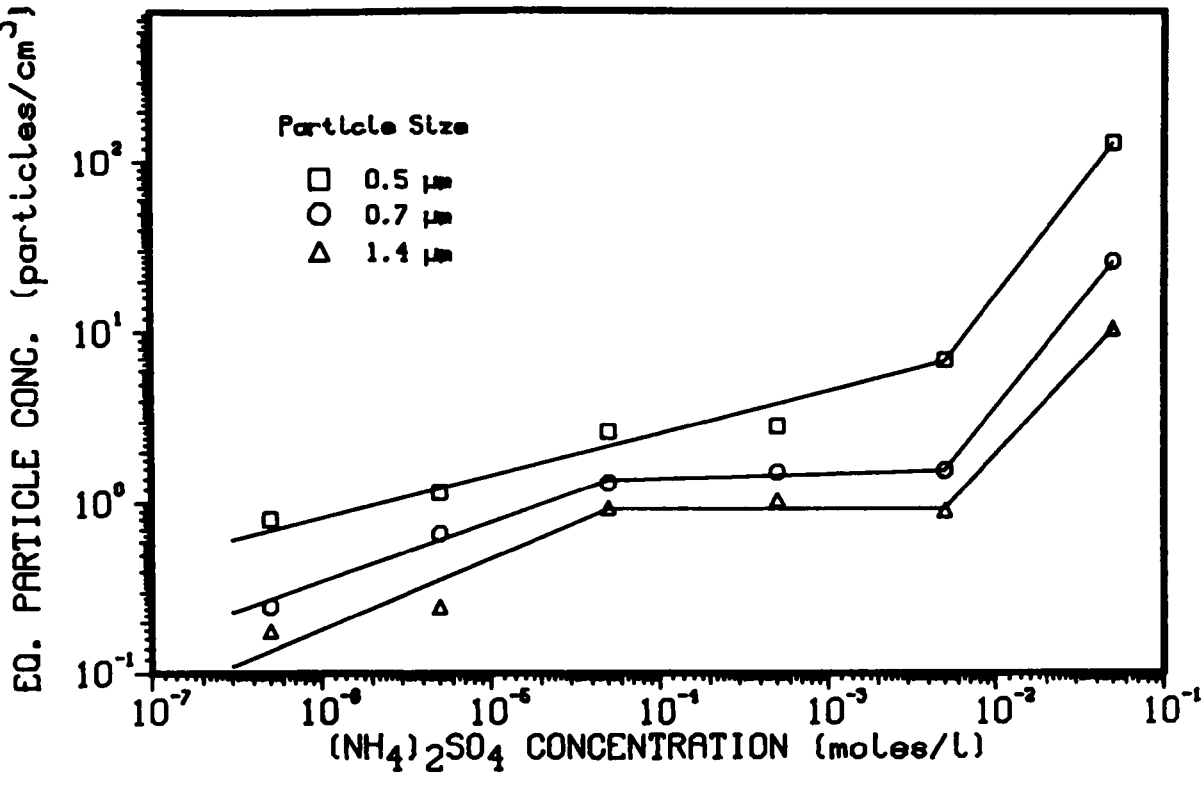

Fig. 6. Effect of $(NH_4)_2SO_4$ Concentration on $(NH_4)_2SO_4$ Particle Size Distribution

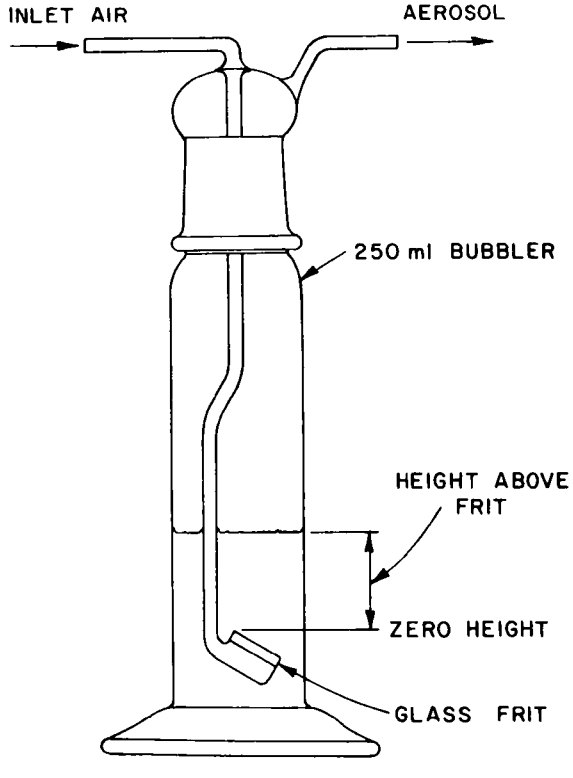

Fig. 7. Diagram of Bubbler and Glass Frit

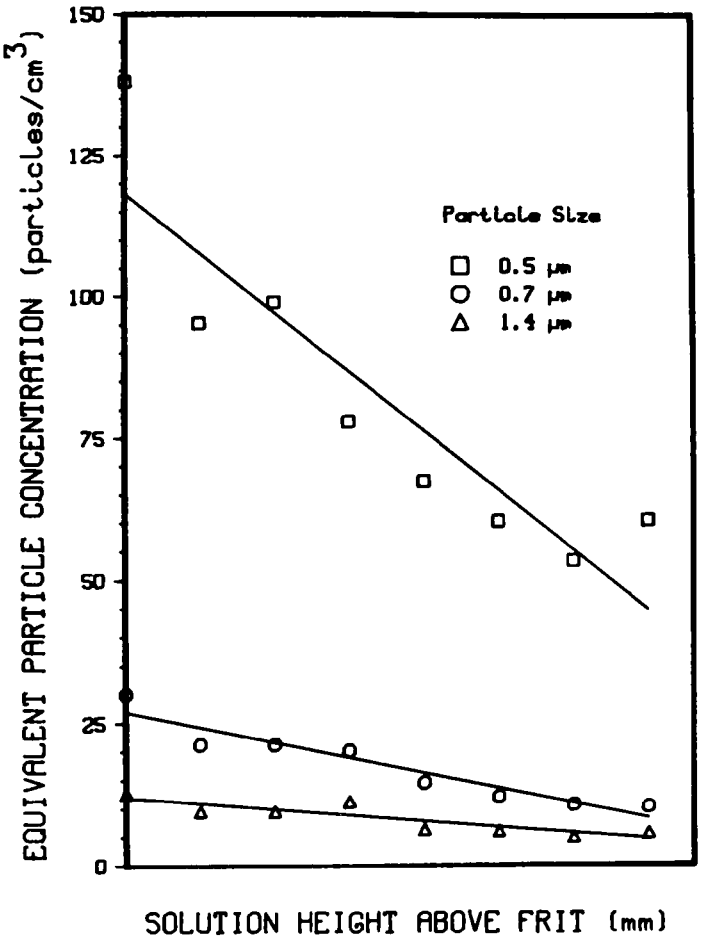

Fig. 8. Effect of Solution Height above Frit on $(NH_4)_2SO_4$ Particle Size Distribution

Effect of frit type on the $(NH_4)_2SO_4$ particle size distribution was also investigated. A coarse and an extra-coarse frit were used. The coarse frit had a maximum pore diameter of 40-60 µm and the extra-coarse frit had a maximum pore diameter between 170 and 220 µm. Figure 9 represents a plot of the $(NH_4)_2SO_4$ size distribution obtained with these two frits. Table 3 gives particle size data for the two frit types. In the size ranges of D_p >3.0 and >5.0 µm, the concentration of aerosol is greater in the case of the extra-coarse frit. This is to be expected since the coarser frit will produce a greater number of larger bubbles. However, in the size ranges of D_p >0.7 and >0.5 µm, the trend is reversed with the coarse frit producing a greater number of fine particles.

Effect of air flow rate through the frit on the particle size distribution of $(NH_4)_2SO_4$ is shown in Figs. 10 and 11. The frits used in the experiments were 20-mm-dia discs. Thus, at an air flow rate of 2.0 L/min, the air flux through the frits was 10.6 $cm^3/(cm^2)(s)$. In these experiments, the air flow rate was varied from 0.5 to 3.0 L/min. The relative humidity in all of these trials was 100%. Figures 10 and 11 contain the upstream and downstream particle-size distribution data as a function of frit air flow rate.

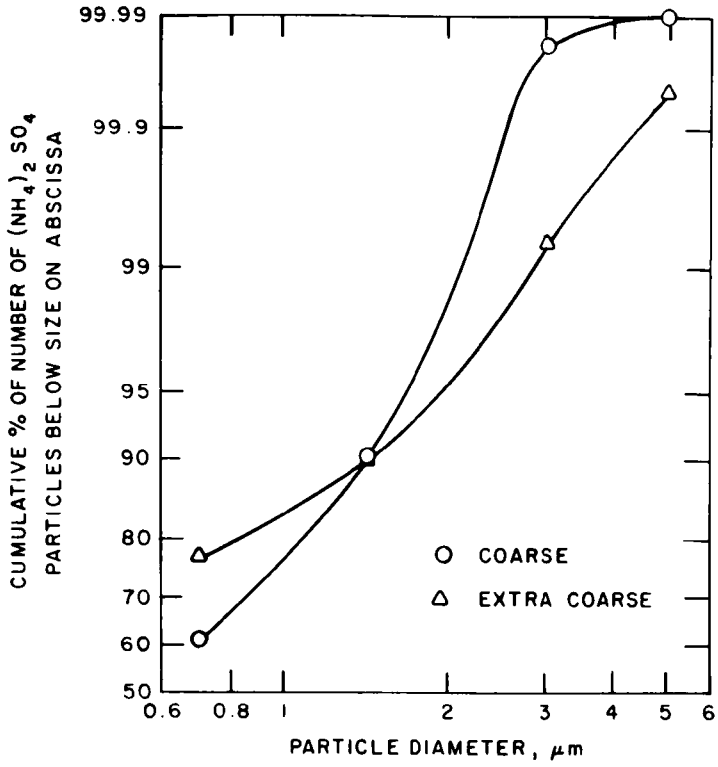

Fig. 9. Effect of Frit Type on Size Distribution of $(NH_4)_2SO_4$ Aerosol

Table 3. Change in $(NH_4)_2SO_4$ Size Distribution with Frit Type (Selected Upstream Data)

	Size Range, μm	Equivalent Particle Concentration, particles/cm^3
Coarse Frit	>0.5	275.0
	>0.7	106.0
	>1.4	28.3
	>3.0	0.04
	>5.0	0.02
Extra Coarse Frit	>0.5	117.0
	>0.7	27.9
	>1.4	12.7
	>3.0	0.78
	>5.0	0.06

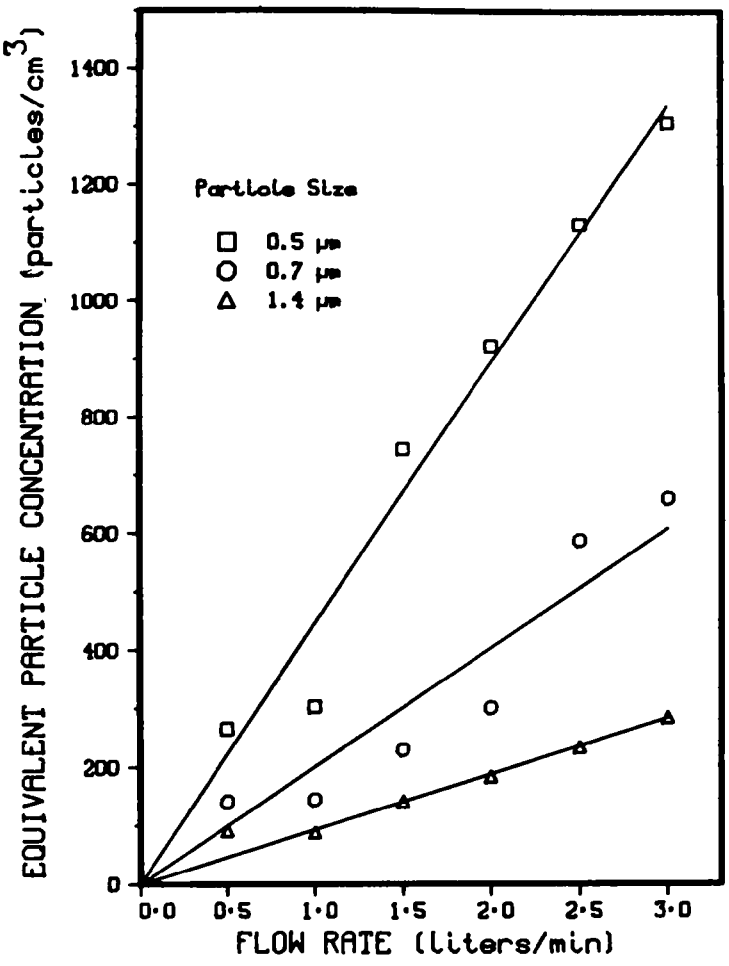

Fig. 10. Effect of Air Flow Rate on the Upstream Equivalent Particle Concentration of $(NH_4)_2SO_4$ Aerosol

Due to particle deposition by sedimentation, the upstream particle concentrations are higher than the downstream particle concentrations in all particle size ranges. Figures 10 and 11 indicate that the majority of particles exist in the <1.4 μm size range. For the upstream data, the equivalent particle concentration increased linearly with flow rate. Figure 11 shows that this linear relationship does not hold for the downstream data. This was probably due to the aging of the aerosol in the flow reactor. For flow rates ≤1.0 L/min, the equivalent particle concentration is less than 50 particles per cm^3. For flow rates >1.5 L/min, the equivalent particle concentration rises sharply, especially for the particle size range D_p >0.5 μm. For both the upstream and downstream data, in the size range D_p >0.5 μm, the equivalent particle concentrations were greater than those for size ranges D_p >0.7 or >1.4 μm. Thus, the coarse frit was more efficient in producing greater numbers of small particles than large particles.

Effect of humidity on the particle size distribution of neutral $(NH_4)_2SO_4$ was also examined. It was found that the size distribution of $(NH_4)_2SO_4$ was not markedly affected by changes in relative humidity below 70%.

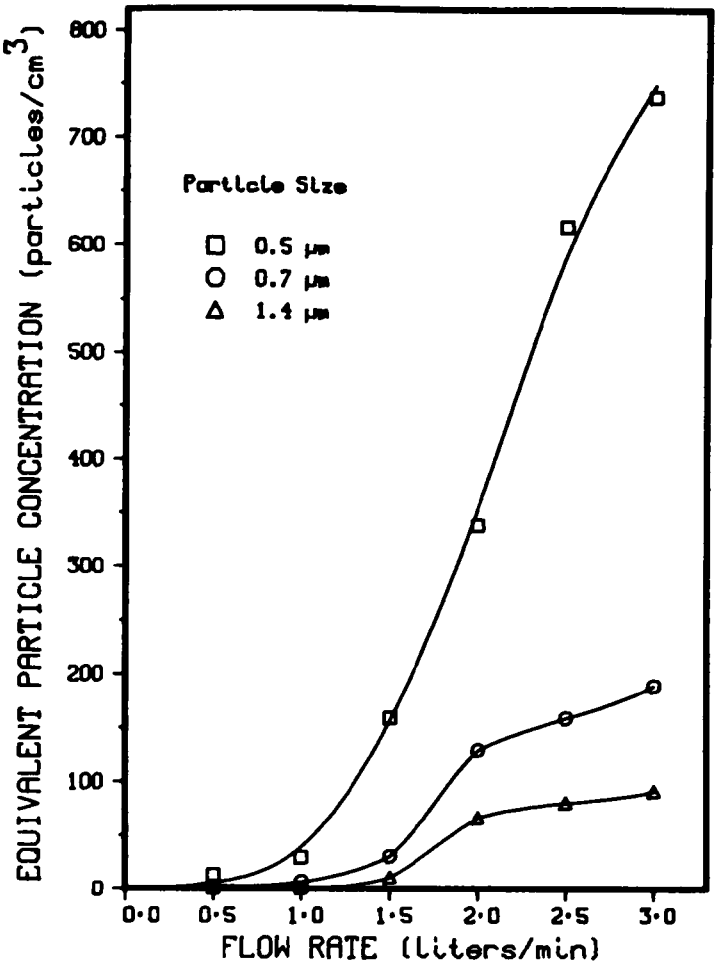

Fig. 11. Effect of Air Flow Rate on the Downstream Equivalent Particle Concentration of $(NH_4)_2SO_4$ Aerosol

In these experiments, the flow rate through the bubblers was kept at a constant 2.0 liters of air per min. The dry air flow rate entering the reactor was varied to produce changes in relative humidity. A Panametrics Model 1000 hygrometer was used to measure the dew point in the flow reactor. The relative humidity was obtained using a psychrometric chart and the dry bulb and dew point temperatures. Figure 12 shows the downstream particle size distribution data obtained in the relative humidity experiments. Two general observations can be made from these findings. It can first be noticed that the vast majority of the particles produced were in the size range D_p <1.4 µm. Experiments conducted at relative humidities from 19 to 71% showed that the size distribution of $(NH_4)_2SO_4$ particles was not markedly affected by changes in relative humidity in this range. According to Charlson,[22] at a relative humidity greater than 65%, $(NH_4)_2SO_4$ aerosol absorbs water vapor and the particle diameter increases. This could explain the relative increase in particle concentrations observed at 100% relative humidity for particle diameters between the detection limit of 0.5 µm and 0.7 µm.

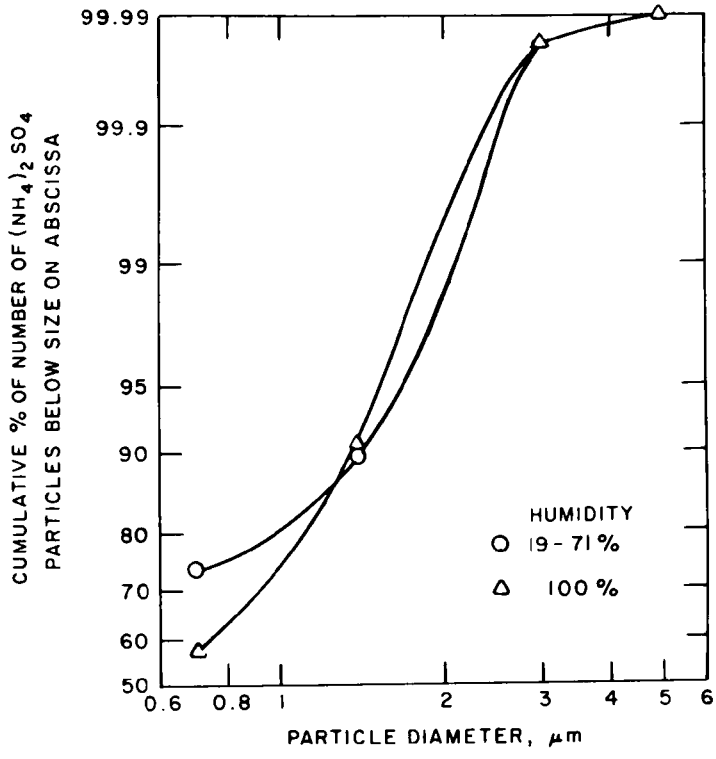

Fig. 12. Effect of Humidity on Size Distribution of $(NH_4)_2SO_4$ Particles Leaving the Flow Reactor

E. Production of Ammonium Bisulfate Aerosols

Efforts were also directed at studying the effects of the various parameters on the size distribution of acidic ammonium sulfate (ammonium bisulfate, NH_4HSO_4) particles. Considerable difficulty was encountered in attempting to generate and maintain an NH_4HSO_4 aerosol in the flow reactor. In several experiments, NH_4HSO_4 was introduced into the flow reactor, but it was determined through infrared spectroscopic analyses that neutral ammonium sulfate [$(NH_4)_2SO_4$] was the only species leaving the flow reactor. Due to the neutralization problem, experiments concerning the effect of humidity and other generation characteristics on the size distribution of NH_4HSO_4 were not feasible. However, the cause of the neutralization was investigated. An infrared spectrum was taken of the NH_4HSO_4 reagent and of the 0.05M NH_4HSO_4 solution prepared from certified reagent grade ammonium bisulfate evaporated to dryness on a hot plate. Both of these spectra matched the upper spectrum shown in Fig. 5. Several procedural changes were made in the experiments which, however, did not eliminate the neutralization problem. These included using deionized-distilled water in all of the bubbler solutions, the overnight addition of an HCl aerosol (generated from 0.01, 0.1, and 1.0M HCl solutions) to neutralize any alkaline residues present in the reactor, and the complete disassembling and thorough cleaning of the flow reactor. Changes involving the molecular sieve system were also made in an attempt to eliminate any ammonia that might be present in the house air stream. The regeneration temperature of the molecular sieves was increased

to 450°C, and one half of the molecular sieves was replaced with activated carbon. The sensitivity limit of the gas chromatographic method used in this work (80 ppm) was too low to detect any ammonia present in the house air stream or the flow reactor. It was suggested that perhaps the molecular sieves were being "overloaded" with H_2O. Experiments conducted with 0.05M and 0.19M phosphoric acid placed upstream from the two H_2O bubblers in an attempt to remove any ammonia from the air stream were also unsuccessful in yielding an acid ammonium sulfate aerosol.

Make-up air is added at the exit of the flow reactor in order to bring the flow rate through the Casella impactor up to the required 17.5 L/min. Thus, the NH_3 present in the make-up air could result in the neutralization of the KBr pellet. HCl aerosol was generated with a 0.5M HCl solution and run through the reactor in an attempt to neutralize any alkaline substances on the walls. A sulfuric acid aerosol was then generated using a 0.1M H_2SO_4 solution. However, an acid ammonium sulfate infrared spectrum was obtained, indicating that ammonia was still present. Generating a sulfuric acid aerosol by placing a 0.25M H_2SO_4 solution in the first and third bubblers and adding dilution air resulted in a sulfuric acid spectrum. The above generation procedure using 0.25M H_2SO_4 was repeated, with nitrogen being used as the carrier gas instead of air. The last two infrared spectra were nearly identical, indicating that the air was not the source of the ammonia. A 0.25M H_2SO_4 solution was placed in the bubbler upstream from the bubbler which contained a 0.1M NH_4HSO_4 solution. In an attempt to fully equilibrate the flow reactor, a bubbler air flow rate of 1.0 L/min was established for 72 h. At the end of this period, the Casella impactor equipped with a KBr disc was used to collect the aerosol sample. (The use of KBr discs, prepared by pressing in an evacuated system, is an accepted procedure for preparing samples for infrared analyses.)[23] Subsequent infrared spectroscopic analysis showed that the sample had been completely neutralized.

After using the vapor from concentrated HCl instead of 1.0M HCl solution to acidify the reactor, the ammonium bisulfate aerosol was maintained in two consecutive experiments with nitrogen as the carrier gas. However, in another seven-hour run, a 0.05M NH_4HSO_4 solution was used with a flow of nitrogen through the bubblers. A glass slide was used in the impactor to collect the aerosol sample instead of KBr pellet. Infrared analysis revealed that the aerosol was completely neutralized during the course of the run (*i.e.*, only $(NH_4)_2SO_4$ was obtained). X-ray diffraction analysis on another portion of the same sample, however, revealed the presence of $(NH_4)_3H(SO_4)_2$ (letovicite). Letovicite appears halfway between $(NH_4)_2SO_4$ and NH_4HSO_4 on the phase diagram. These differences in analyses indicated that the sample was only partially neutralized and that some neutralization could have taken place during the milling procedure[23] for the infrared analyses. However, no milling procedure problems were encountered when H_2SO_4 samples from the flow reactor were processed. One conlcusion that can be reached from this group of experiments is that this flow reactor system could not reliably generate and deliver a non-neutral aerosol.

F. Generation of Metal-Bearing Aerosols

Several methods for generating metal-bearing aerosols have been reported in the literature. These include sublimiation of the metal or oxide followed by condensation of the vapor,[24] using a combustible gas flame together with an atomized metallic salt solution,[25] and passing a salt solution aerosol through a furnace.[26]

In the present study, metal-bearing aerosols were generated by the combustion of metallic salt solutions in alcohols. Initially, saturated solutions of zinc, copper, and manganese acetates were prepared with n-butyl alcohol. The combustor consisted of an alcohol lamp burning in an enclosure. After passage of the combustion-generated aerosol through the flow reactor, only the zinc acetate was detected on the Millipore filter by X-ray diffraction. This was probably due to the solubility characteristics of the various acetates in the alcoholic solutions. Other alcohols of lower molecular weight than butanol were also used in an effort to increase the acetate solubilities, but experimental difficulties keeping the alcohol lamp burning precluded their use.

A series of experiments was conducted using zinc acetate dissolved in 100% n-butyl alcohol, as well as 75% butanol and 25% propanol. Samples were collected upstream and downstream of the flow reactor with only air flowing through the combustor, with an $(NH_4)_2SO_4$ aerosol combined with the metal aerosol in the combustor. Samples were also collected downstream of the flow reactor with an $(NH_4)_2SO_4$ aerosol combined with the metal aerosol in the flow reactor. In addition to a Fluoropore filter (pore size, 1.0 μm), the Casella impactor equipped with glass slides was used to collect the samples. The samples were dissolved in nitric acid and analyzed using atomic absorption spectroscopy. The summary of results of the atomic absorption analyses are presented in Table 4. In the measurements conducted upstream of the flow reactor, the impactor was not used to collect the samples since the air flow rate through the combustor alone was much less than the 17 L/min required for proper operation of the impactor.

In experiment MA-1, clean air was introduced into the combustor at a flow rate of 5.5 L/min. After 2.5 h of operation, 0.6 μg of zinc was collected on the filter placed upstream of the flow reactor. In run MA-2, 5 L/min of clean air and 1.5 L/min of air containing $(NH_4)_2SO_4$ aerosol were introduced into the combustor. In 2.5 h, 35.1 μg of zinc were collected on the filter, indicating that either the $(NH_4)_2SO_4$ particles were serving as condensation nuclei for the metal aerosol, or that the collected $(NH_4)_2SO_4$ was acting as a filter cake to filter out the fine metal aerosol particles. The combustion aerosol itself was <0.5 μm in diameter. This was shown by connecting the optical particle counter immediately downstream from the combustor when no change above the background count was obtained.

This method of aerosol generation, however, showed marked variability in the aerosols produced. For example, in run MA-3, 5.5 L/min of clean air were introduced into the combustor. Downstream of the flow reactor, 1.1 μg of zinc were collected on the impactor and 36.8 μg were collected on the filter in 2.5 h. However, under identical conditions, run MA-4 yielded 6.9 μg of zinc on the impactor and 6.3 μg on the filter in 2.5 h. Thus, not only was the rate of zinc aerosol production different in the two runs, the aerosol size distribution was also different, with relatively coarser aerosol particles being produced in run MA-4.

Table 4. Summary of Data from the Zinc Aerosol Experiments

Run No.	Conditions[a]	Sampling Location	A Wt. of Zinc on Impactor, µg	B Wt. of Zinc on Filter, µg	$\frac{A}{A+B}$, %
MA-1	5.5 L air/min through combustor [b]	Upstream	--	0.6	--
MA-2	5.0 L/min of clean air and 1.5 L/min of air containing $(NH_4)_2SO_4$ aerosol combined in the combustor	Upstream	--	35.1	--
MA-3	5.5 L/min of clean air through combustor	Downstream	1.1	36.8	2.9
MA-4	Same as for Run MA-3	Downstream	6.9	6.3	52.3
MA-5(1)	5.5 L/min of clean air through combustor	Downstream	5.1	15.7	24.5
MA-5(2)	5.5 L/min of clean air through combustor and 1.0 L/min of air containing $(NH_4)_2SO_4$ aerosol combined in the reactor	Downstream	1.7	5.5	23.6
MA-6	5.0 L/min of clean air and 1.5 L/min of air containing $(NH_4)_2SO_4$ aerosol combined in the combustor	Downstream	2.4	56.2	4.1
MA-7(1)	5.5 L/min of clean air through combustor [c]	Downstream	3.5	2.4	59.3
MA-7(2)	5.5 L/min of clean air through combustor and 1.0 L/min of air containing $(NH_4)_2SO_4$. aerosol combined in the reactor	Downstream	1.6	8.1	16.5

[a] Aerosol collection time of 2.5 h in each run or part of run.

[b] Runs enclosed in brackets were performed consecutively on the same day.

[c] In this run, the zinc acetate was dissolved in a mixture of 75% butanol-25% propanol. In all other experiments, the zinc acetate was dissolved in pure butanol.

However, experiments were conducted to examine the behavior of zinc aerosols in the presence of $(NH_4)_2SO_4$ aerosols. In one type of experiment, the air stream from the combustor was combined with an $(NH_4)_2SO_4$ aerosol stream in the flow reactor to investigate coagulation of the zinc and $(NH_4)_2SO_4$ particles (run MA-5). In a second type of experiment, the ammonium sulfate aerosol was introduced into the combustor, so that the $(NH_4)_2SO_4$ particles could act as condensation nuclei for the zinc acetate-alcohol combustion products (run MA-6). In the first part of run MA-5, an air flow rate of 5.5 L/min was established through the combustor and impactor and filter samples collected downstream of the flow reactor for 2.5 h. In the second part of run MA-5, an additional 1.0 L/min of air containing $(NH_4)_2SO_4$ aerosol was added at the flow reactor inlet, and the downstream samples collected for another 2.5 h. A comparison of the sampling results for the two parts of run MA-5 shows that, although the total amount of zinc aerosolized was different, the particle size distribution was not significantly affected by the presence of the $(NH_4)_2SO_4$ aerosol in the flow reactor. In part one of run MA-5, 24.5% of the zinc aerosol was greater than 0.45 μm in particle diameter (since this is the cut-off diameter for the fourth stage of the Casella impactor), while in part two, 23.6% of the zinc aerosol was made up of particles greater than 0.45 μm. In run MA-6, where the $(NH_4)_2SO_4$ particles were present in the combustor, the total amount of zinc aerosolized in 2.5 h was greater than in previous experiments, but only 4.1% of the zinc was in particles greater than 0.45 μm in diameter. Because of the non-reproducibility of this aerosol generation system, no firm conclusions could be drawn from these experiments. However, the ammonium sulfate aerosol apparently had no significant influence on the zinc aerosol.

An increase in the zinc aerosol concentration was attempted by using a 75% butanol-25% propanol mixture as the solvent for zinc acetate, rather than pure butanol, as used in the above experiments. The presence of the lighter alcohol should result in increased zinc acetate solubility, leading to a higher concentration of zinc in the flame. Run MA-7 was conducted in two parts, similar to run MA-5. However, as shown in Table 4, the amounts of aerosolized zinc collected in 2.5 h were still very low.

G. Generation of Organic Material Aerosols

Organic aerosols were generated by sublimation and subsequent cooling of the vapor. Naphthalene, which has been identified as a product of coal combustion, can be considered to be a representative polycyclic aromatic hydrocarbon.[17] In the first effort to generate a naphthalene aerosol, sublimation at room temperature was tried; however, only 5.0 μg of naphthalene was collected in 2.5 h on a Fluoropore filter (1.0-μm pore diameter) placed at the exit of the flow reactor. (The filter samples were dissolved in carbon tetrachloride and analyzed using gas chromatography.) In order to increase the yield, heating tape was used to heat the air before it reached the naphthalene. The naphthalene was placed in an open petri dish and allowed to sublime in the heated air. The air temperature in the vaporizer was 39°C. In this case, the yield on the filter was 8.7 μg in 2.5 h. Because naphthalene is quite volatile (b.p. 218°C), it was thought that some of the naphthalene was being revaporized after being trapped by the filter. Acenaphthalene (Aldrich Chemical Co., 99% assay, b.p. 280°C) is

less volatile and thus had an increased likelihood of not being revaporized after being collected on the filter. As above, the filter samples were dissolved in carbon tetrachloride and analyzed using gas chromatography. In one experiment, using heated air as described above, 1.0 μg of acenaphthalene was collected on the filter placed downstream of the flow reactor. However, upstream of the flow reactor, 15.3 μg of acenaphthalene was collected on the Fluoropore filter and 40.7 μg of acenaphthalene was collected on the filter's fibrous support in a subsequent experiment.

In the next series of experiments, a brass block wrapped in heating tape was used as a heating device in the vaporizer in lieu of the heating tape on the inlet air line. The acenaphthalene was placed in a 10-cm^3 beaker located on the brass block. In one experiment, the air temperature in the vaporizer was 47°C and the temperature of the melted acenaphthalene was 88°C. Gas chromatographic analyses revealed that the filter placed at the downstream end of the flow reactor contained 2.37 μg and the fibrous support, 1.0 μg of acenaphthalene. In a subsequent experiment, 1.5 L/min of $(NH_4)_2SO_4$ aerosol containing air was added to the vaporizer, and 7.8 μg was collected on the filter and 2.8 μg on the fibrous support. These two values were about three times greater than in the preceding run. In another run in which the acenaphthalene and $(NH_4)_2SO_4$ aerosol were combined in the reactor, the results were approximately the same as those for the case in which the $(NH_4)_2SO_4$ aerosol was added to the vaporizer. In these runs, the ammonium sulfate aerosol was acting as a filter cake or the $(NH_4)_2SO_4$ particles were serving as condensation nuclei for the organic aerosol. In general, the amount of acenaphthalene deposited on the impactor slide was < 0.2 μg. This indicated that coagulation was not taking place between the $(NH_4)_2SO_4$ aerosol and the acenaphthalene aerosol. In these experiments, the tygon tubing that led from the condenser to the stainless steel reactor inlet line turned yellow. This was believed to be a phenomenon of diffusional deposition of the very fine aerosol of acenaphthalene, which is yellow in color.

VI. CONCLUSIONS

Results of the mass balance experiment indicated mass loss in transit through the flow reactor of 23.0 ± 3.5%. The average percent loss in equivalent particle concentration was 24.9%, which agrees closely with the above value. The major factor contributing to the above losses was sedimentation.

Several factors affecting aerosol generation in the bubbler system were investigated. As the solution concentration increased, the equivalent particle concentration also increased. The equivalent particle concentration decreased as the solution height above the frit increased. This could be accounted for by the increased solution depth affording more time for the bubbles to coalesce. Frit type influenced the particle-size distribution generated, with a coarse frit producing an increased concentration of aerosol in the size range $D_p > 1.4$ μm. As the flow rate of air through the frit increased, the equivalent particle concentration also increased. Below 70% relative humidity, no effect on the particle size distribution of neutral ammonium sulfate was observed with variations in relative humidity. Above

70% relative humidity, the equivalent particle concentrations increased in the size range $D_p \geq 0.5$ μm, presumably due to absorption of water vapor and subsequent increase in particle diameter. From the problems encountered with neutralization of ammonium bisulfate and sulfuric acid aerosols, it was concluded that the flow reactor system in its present configuration could not reliably generate an aged, non-neutral aerosol.

Metal containing aerosols (*e.g.*, zinc) can be readily generated. However, further work is needed to ensure the reproducibility of the aerosol composition and concentration. With slight modifications of the flow reactor system, an organic areosol of acenaphthalene was generated. Further studies are needed, however, to assess the applicability of the flow reactor to a wider spectrum of organic compounds.

APPENDIX

AEROSOL REMOVAL RATES

Removal by Diffusional Deposition

The magnitude of diffusional deposition in the flow reactor was calculated theoretically. The decrease in particle concentration due to diffusional deposition on the walls of a cylinder was calculated from a nomograph (Fig. 6.8, Ref. 20). The parameters considered were:

D_p = particle diameter

l = tube length = 350 cm

V_f = mean flow velocity in the tube (15.24-cm-dia, 4 L/min flow rate) = 0.365 cm/s

R = radius of tube = 7.62 cm

p = atmospheric pressure = 760 torr

n = number concentration at the tube exit

n_o = inlet number concentration

For a particle diameter of 0.5 μm, $n/n_o = 0.999$. For a particle diameter of 5.0 μm, $n/n_o = 0.99$. Thus, under the above conditions, diffusional deposition effects in the flow reactor can be neglected.

Removal by Sedimentation

The magnitude of the deposition of particles by sedimentation in the flow reactor was calculated theoretically. The gravitational settling losses of particles flowing through a horizontal cylindrical tube under laminar flow conditions can be calculated from the following equation:[20]

$$n/n_o = \exp\left[\frac{-2V_s l}{\pi V_f R}\right] \tag{1}$$

where

V_s = settling velocity of particle, defined by

$$V_s = \frac{(\rho_p - \rho_f) g D_p^2}{18 \mu_f} \tag{2}$$

where

ρ_f = density of fluid medium

ρ_p = density of the particle

μ_f = coefficient of viscosity of the fluid medium

For sedimentation in air, ρ_f is usually negligible compared to ρ_p. Assume that ρ_p = 1 g/cm^3 and D_p = 0.7 μm, and with μ_f = 0.018 centipoise for air at 75°F. Substituting these values in Eq. 2, $V_s = 1.48 \times 10^{-3}$ cm/s. Using the derived value for V_s and the values listed above for l, R, and V_f, Eq. 1 yields

$$n/n_o = 0.888 \text{ for } D_p = 0.7 \ \mu m$$

For other particle diameters, the settling velocities, V_s, and the number concentration ratios, n/n_o, were calculated to be:

D_p, μm	V_s, cm/s	n/n_o
0.5	7.56×10^{-4}	0.941
1.4	5.93×10^{-3}	0.622
3.0	2.72×10^{-2}	0.113
5.0	7.56×10^{-2}	0.002

Thus, under conditions specified above, deposition by sedimentation in the flow reactor is not negligible.

Removal by Particle Coagulation

The magnitude of particle coagulation in the flow reactor was calculated theoretically from the following equation:[21]

$$\frac{dn}{dt} = -K_o n^2 \tag{3}$$

Integration of Eq. 3 yields:

$$\frac{1}{n} - \frac{1}{n_o} = K_o t \text{ or } \frac{n}{n_o} = 1 - nK_o t \tag{4}$$

where t is time and K_o is the coagulation constant. For a particle 0.5 μm in diameter, $K_o = 4.06 \times 10^{-10}$ cm^3/s. From Table 3, the particle number concentration of the >0.5-μm-dia particles is 300 particles per cm^3 or less. The residence time in the flow reactor is about 15 min. Then, from Eq. 4, for D_p = 0.5 μm, n/n_o = 0.999, *i.e.*, removal by coagulation can be neglected.

REFERENCES

1. D. H. Slade, Chemist/Meteorologist Workshop 1975, ERDA 1217-75, Ft. Lauderdale, FL, pp. 70, 75 (January 1975).

2. R. A. McCormick and J. H. Ludwig, *Climate Modification by Atmospheric Aerosols*, Science 156, 1358-1359 (1967),

3. E. Robinson and R. C. Robbins, *Sources, Abundance and Fate of Gaseous Atmospheric Pollutants*, Stanford Research Institute, Menlo Park, CA, Prepared for American Petroleum Institute, New York, NY (February 1968).

4. *Summary Report on Suspended Sulfates and Sulfuric Acid Aerosols*, U. S. Environmental Protection Agency, Research Triangle Park, NC (unpublished) (May 14, 1974).

5. W. W. Kellog, *The Sulfur Cycle*, Science 175, 587-596 (1972).

6. M. O. Amdur, *Toxicologic Appraisal of Particulate Matter, Oxides of Sulfur, and Sulfuric Acid*, J. Air Pollut. Contr. Assoc. 19(9), 638-644 (September 1969).

7. *Currents*, Environ. Sci. and Technol. 10(12), 1077 (November 1976).

8. K. T. Whitby, *The Aerosol Size Distribution of Los Angeles Smog*, J. Colloid Interface Sci. 39(1), 177-204 (April 1972).

9. K. T. Whitby and B. Y. H. Liu, *Advances in Instrumentation and Techniques for Aerosol Generation and Measurement*, University of Minnesota, Minneapolis, MN (unpublished) (1974).

10. *Position Paper on Regulation of Atmospheric Sulfates*, EPA-450/2-75-007, United States Environmental Protection Agency, Research Triangle Park, NC, pp. 2, 13, 22-24, 27-34, 36 (September 1975).

11. *Mineral Resources and the Environment*, Committee on Mineral Resources and the Environment, the Commission on Natural Resources, and the National Research Council, National Academy of Sciences, Washington, DC, pp. 227, 229, 240 ff (March 1975).

12. *National Strategy for Control of Sulfur Oxides from Electric Power Plants*, U. S. Environmental Protection Agency, Washington, DC (July 10, 1974).

13. A. Yves, *Long Term Continuous Exposure to Sulfuric Acid Mist in Cynomologus Monkeys and Guinea Pigs*, Arch. Environ. Health 27, 16 (1973).

14. *Analysis of the Automotive Sulfate Question--Summary of Findings*, Energy and Environmental Analysis, Inc., Arlington, VA 18 (no data).

15. *Threshold Limit Values for Chemical Substances and Physical Agents in the Workroom Environment with Intended Changes for 1974*, American Conference of Governmental Industrial Hygienists, Cincinnati, OH (1974).

16. M. O. Amdur, *The Irritant Potency of Zinc Ammonium Sulfate of Different Particles Sizes*, Am. Ind. Hyg. Assoc. J. 24, 326-333 (1963).

17. A. Stern, *Air Pollution*, Vol. I, Academic Press, New York, NY, pp. 146-147, 150, 152 (1976).

18. A. Stern, *Air Pollution*, Vol. II, Academic Press, New York, NY, pp. 187-196 (1968).

19. B. Y. H. Liu, Ed., *Fine Particles*, Academic Press, New York, NY, pp. 235-252 (1976).

20. Richard Dennis, Ed., *Handbook on Aerosols*, ERDA, TID-26608, Springfield, VA, pp. 125-127, 159-168 (1976).

21. N. A. Fuchs, *The Mechanics of Aerosols*, Pergamon Press, Oxford, England, pp. 290-291 (1964).

22. R. J. Charlson, *$H_2SO_4/(NH_4)_2SO_4$ Background Aerosol: Optical Detection in the Saint Louis Region*, Atmos. Environ. 8(12), 1257-1267 (December 1974).

23. Werner Brügel, *An Introduction to Infrared Spectroscopy*, John Wiley & Sons, Inc., New York, NY, pp. 231-240 (1962).

24. H. P. Brodia, *Studies of Small Metallic Particles Formed by Homogeneous Nucleation: Light Scattering and Electron Microscopy*, Environmental Protection Agency, Washington, DC, EPA-650/3-75-006, pp. 5, 20 (February 1975).

25. B. S. Marshall, *A Field Method for the Determination of Zinc Oxide Fume in Air*, Analyst 96, 569-578 (August 1971).

26. W. L. Dyson, *Reactivity of Zinc Oxide Fume with Sulfur Dioxide in Air*, Environ. Sci. and Technol. 10(5), 476-481 (May 1976).

Distribution for ANL-77-90

Internal:

M. V. Nevitt
J. A. Kyger
A. Amorosi
R. Avery
D. W. Cissel
S. A. Davis
B. R. T. Frost
D. C. Rardin
R. G. Staker
R. J. Teunis
C. E. Till
R. S. Zeno
H. O. Monson
P. R. Fields
J. S. Bogard
L. Burris (4)
F. A. Cafasso
P. T. Cunningham (2)
B. D. Holt
B. R. Hubble
H. R. Isaacson
S. A. Johnson (2)
G. M. Kesser
R. Kumar (5)
A. F. Melton
E. L. Nielsen
A. B. Krisciunas
ANL Contract File
ANL Libraries (5)
TIS Files (6)

External:

DOE-TIC, for distribution per UC-4 (198)
Manager, Chicago Operations Office
Chief, Chicago Patent Group
President, Argonne Universities Association
Chemical Engineering Division Review Committee:
  R. C. Axtmann, Princeton U.
  R. E. Balzhiser, Electric Power Research Institute
  J. T. Banchero, U. Notre Dame
  D. L. Douglas, Gould Inc.
  P. W. Gilles, U. Kansas
  R. I. Newman, Allied Chemical Corp.
  G. M. Rosenblatt, Pennsylvania State U.
J. E. Ainsworth, Lawrence Berkeley Lab.
J. E. Etzel, Purdue U.
R. B. Jacko, Purdue U.
R. W. Zygmunt, Mobil Oil Co., Joliet, Ill. (10)